CYCLONE STRUCTURAL TESTING STATION
JAMES COOK UNIVERSITY OF NORTH QUEENSLAND

COMPARISON OF WIND PRESSURE AND FATIGUE DAMAGE TO HIP AND GABLE ROOF CLADDINGS

by

Y. L. Xu
G. F. Reardon
J. A. Mahlberg
D. J. Henderson

TECHNICAL REPORT NO. 43

September 1996

Xu, Y. L. (You Lin), 1952-
Comparison of wind pressure and fatigue damage to hip and gable roof claddings.

Bibliography.
ISBN 0 86443 606 8
ISSN 0158 - 8338.

1. Building, Stormproof. 2. Roofing, Iron and steel - Testing. 3. Roofs - Aerodynamics. 4. Wind-pressure. I. James Cook University of North Queensland, Cyclone Structural Testing Station. II Title. (Series: Technical Report (James Cook University of North Queensland, Cyclone Structural Testing Station) ; no 43).

624.176

CONTENTS

COMPARISON OF WIND PRESSURE AND FATIGUE DAMAGE TO HIP AND GABLE ROOF CLADDINGS

Synopsis

A number of post disaster investigations on wind-induced damage to low-rise buildings and houses have revealed that hip roofs have better performance than gable roofs during strong winds. Limited wind tunnel studies also showed that local negative peak pressures on gable roofs could be roughly 50 % greater than those on hip roofs. These results have stimulated the present study to compare wind-induced pressures, fatigue loading, and fatigue damage to hip and gable roof claddings using wind tunnel test techniques and computer analyses.

The magnitude and distribution of wind pressures on both roofs are first measured at different wind directions. Fatigue characteristics of wind pressures are then identified based on a rainflow count method for each tap at its critical wind direction in which its largest negative pressure occurs. Total fatigue loading at each tap on both roofs is then computed using the obtained fatigue characteristics and information on wind climate. Finally, fatigue damage to screw-fastened light-gauge steel roof sheetings of different profiles is estimated in terms of previously-obtained S-N curves and a modified Miner's rule.

The distributions of peak pressure coefficient and fatigue damage index over both roofs show that under the same strong winds, peak pressures and fatigue damage to the hip roof cladding is much less severe than those to the gable roof cladding. For each type of roof configuration, there are considerable differences in fatigue loading and fatigue damage with respect to different locations of pressure taps and different profiles of roof sheetings.

1 INTRODUCTION

Wind pressures on roof claddings of houses and low-rise buildings are heavily fluctuating due to the natural turbulence in incident wind near the ground and the turbulence induced by flow-building interaction. Thus, sustained strong winds can cause severe fatigue damage to light-gauge steel roof claddings. This has been well documented for Cyclone Tracy (Walker, 1975) and others.

There are many types of roof configurations used in house and low-rise building construction. A number of post disaster investigations on wind-induced damage to structures (e.g., Wittenoom, 1975) have revealed that hip roofs have better performance than gable roofs during strong winds. Sparks et. al. (1988) measured mean wind pressures on both types of roofs using wind tunnel testing techniques with the aim of predicting the risk of structural damage associated with roof configurations. Meecham et. al. (1991) studied in detail the magnitude and distribution of both mean and peak pressures and related them to the structural framing of each type of roof. Their results showed that the distribution of wind pressures on hip roofs was significantly different from that on gable roofs. Local negative peak pressures on a gable roof could be roughly 50 % greater than those on a hip roof. These research activities have stimulated the present study to compare wind-induced pressures, fatigue loading, and fatigue damage to hip and gable roof claddings.

Since full-scale wind pressure records on both hip and gable roofs of otherwise similar geometry are not available to the writers, wind tunnel tests have to be used to obtain the required roof pressure records. A model- and full-scale comparison of fatigue-related characteristics of wind pressures on the Texas Tech Experimental Building has been therefore conducted before the present study (Xu and Reardon 1995). The comparative study showed that there was reasonable agreement about the number of cycles and cycle histogram when the cut-off frequency, sampling frequency and length used in the model test were equivalent to those used in the full-scale test. The negative peak pressure coefficients at the roof corner were however underestimated by the model-scale test to some extent. While the difference in the local negative peak pressures requires further study (in fact, many researchers in wind engineering are actively investigating this kind of difference), the results obtained from the present study are believed to be meaningful because it is mainly a comparative study between two roof configurations.

All dimensions in mm

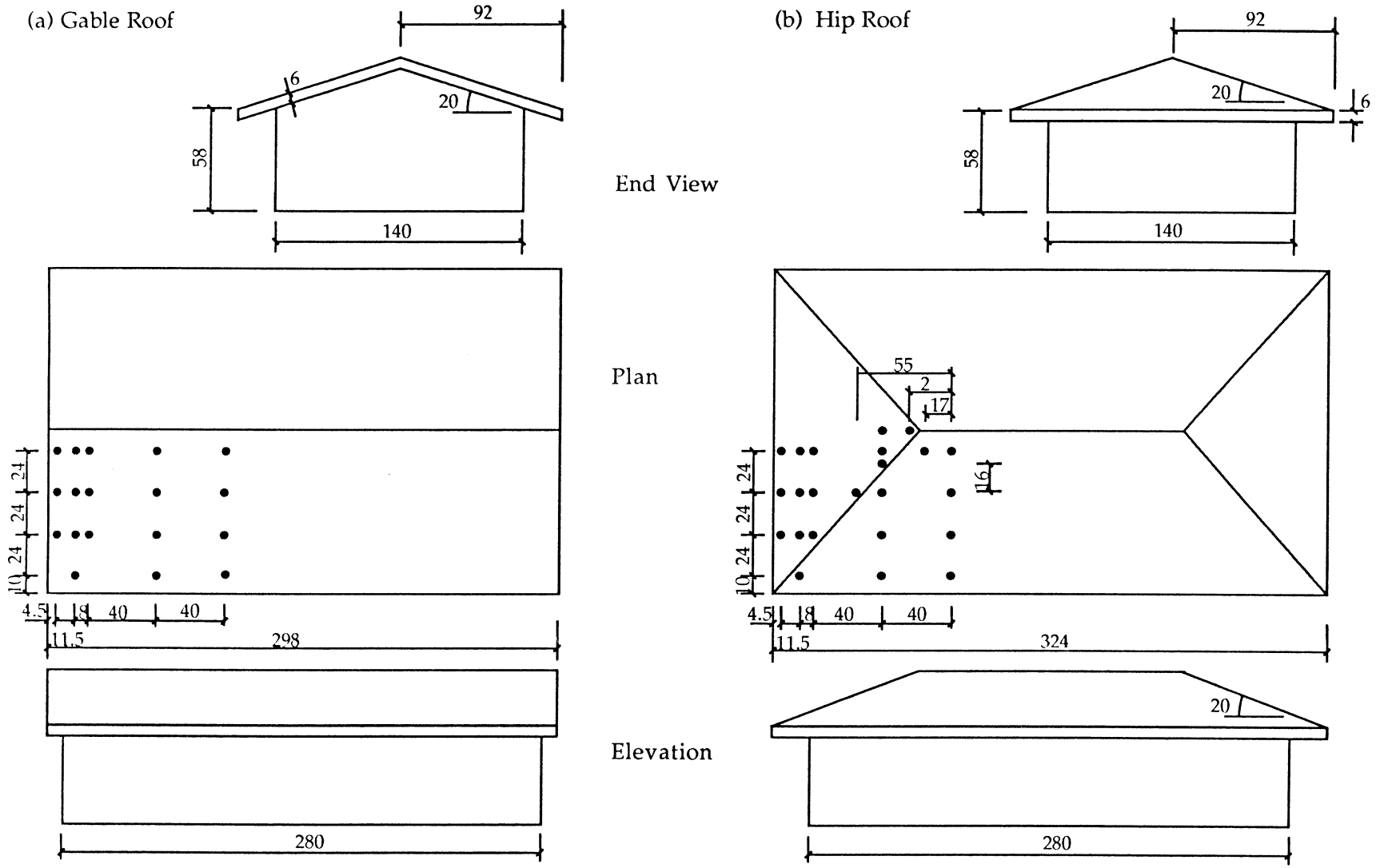

FIG. 1 MODEL CONFIGURATIONS AND PRESSURE TAP LOCATIONS

2 EXPERIMENTAL ARRANGEMENT

2.1 Wind Tunnel and Flow Simulation

The experiments were carried out in the boundary layer wind tunnel of James Cook University. The wind tunnel has been described previously by Holmes in detail (1980). Briefly, it is of open-circuit configuration with an axial-flow fan mounted downwind of the working section. The working section is 17.5 m long, 2.5 m wide, and 2.0 m high.

A 1:50 scale model of natural wind was developed in the wind tunnel to simulate the natural wind over open-country terrain. The flow simulation technique mainly consisted of mounting a 400 mm high single plain fence spanning the floor at the start of the test section and covering the whole working section with low-pile carpet. The mean longitudinal wind speed profile measured in the wind tunnel was in good agreement with the power law of an exponent 0.14. The mean wind speed measured at the 58 mm eaves height of the building model was 10.1 m/s. The longitudinal turbulence intensity measured at the eaves height was about 0.2. The integral length of longitudinal turbulence measured at the eaves height was about 40 m. Compared with the full-scale integral length from the von-Karman spectrum at the same terrain, there was a small distortion of a factor of 1.27 in the scale of turbulence.

2.2 Building Models

Two building models with large overhangs were made at a geometric scale of 1:50: one with a gable roof, and the other with a hip roof (Fig. 1). A 20^0 roof pitch was selected for both building models because it is one of the most common roof pitches in use, and also the highest mean and instantaneous peak suctions occur on the 20^0 pitch roof in the gable roof case as Holmes (1981) observed. The aspect ratio of the two buildings (length to width) was chosen as 2:1. The eaves height was 58 mm in model scale (2.9 m in full scale). Since the overhang at the gable end is usually shorter than the overhang in the front or back wall in practice, the total length of the hip roof model made in this study was slightly longer than the total length of the gable roof model (Fig. 1). Considering vortex shedding often generated at leading edges, the roof edges of both buildings were taken as a reference to the location of pressure taps. The distance of each tap along the width of the models shown in Fig. 1 referred to the sloping surface of the roof. Because of the symmetric conditions of the models, a total of 18 taps were arranged

on a quarter of the gable roof, and a total of 23 taps were on a quarter of the hip roof. All the taps were numbered in Fig. 2 for the convenience of later explanation of test results. The building models were tested at a 15^0 increment from 0^0 to 180^0 and then a 30^0 increment from 180^0 to 360^0 with respect to the central line of the model (Fig. 2).

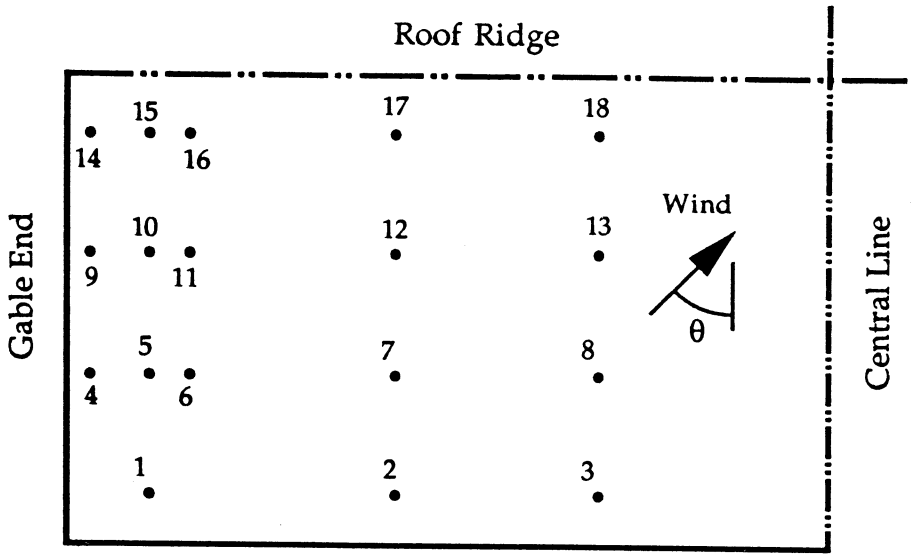

(a) Gable Roof

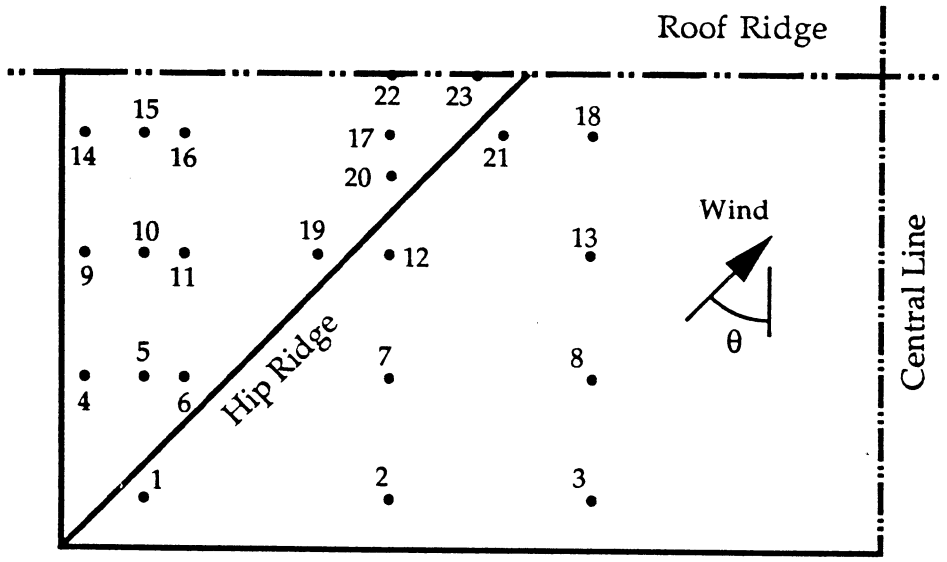

(b) Hip Roof

FIG.2 PRESSURE TAP NUMBERS

2.3 Instrumentation and Measurement

The building models were constructed from 6 mm thick "perspex" sheet. The pressure taps consisted of 10 mm long pieces of 1.6 external diameter stainless-steel tubing inserted in holes drilled in the "perspex", with one end of the tubing flush with the roof surface. Pressure measurement was carried out using two Honeywell 163 pressure transducers mounted within 48 port "Scanivalves". The pressure taps on the models were connected to the "Scanivalves" by 450 mm long pieces of 1.6 mm internal diameter vinyl tubing with two 0.3 mm internal diameter restricters placed along the tubing. This pressure measurement system gave a linear frequency response up to 100 Hz and a gradual attenuation from 100 Hz to about 300 Hz with a "half power" point.

The reference velocity was taken during all experimental runs at the eaves height of the models and was used to calculate pressure coefficients. The static pressure was taken from the static holes of a pitot static tube mounted at 1 m above the floor during each run and was then converted to the static pressure at the eaves height in terms of a profile of static pressure previously measured through the boundary layer of the wind tunnel.

The signals from the transducers were low-pass filtered at 250 Hz and were digitally sampled using a Data 6000 analyser. The sampling frequency was 1000 Hz and the sampling duration of each run was 32 seconds. The mean, root mean square (rms), minimum and maximum peak pressure coefficients were calculated using a mini-computer based on the average of five runs.

The aforementioned pressure measurement system was used to detect the critical wind direction for each tap where its largest negative peak pressure occurred. When storing the pressure time history at the critical wind direction for each tap for later fatigue loading analysis, the pressure measurement system consisted of the tubing and transducer only, i.e., without "Scanivalves" being included. The constant frequency response of this pressure measurement system was up to 230 Hz. The higher system frequency response is desirable to identify fatigue characteristics of wind pressures.

3 COMPARISON OF PRESSURE COEFFICIENTS

Wind pressure coefficients expressed here are in the form of

$$C_p = \frac{p - p_o}{(\frac{1}{2}\rho \bar{u}_r^2)} \quad (1)$$

where p = the pressure; p_o = the static pressure at the eaves height: $\bar{u}_r$ = the mean longitudinal wind speed at the eaves height; and ρ = the air density. Equation 1 is used to derive the mean, root mean square (rms), maximum and minimum peak pressure coefficients.

3.1 Mean Pressure Coefficients

The spatial distribution of mean pressure coefficient on the gable roof for the 0^0 wind direction is shown in Fig. 3 (a). It is seen that all roof pressures have a negative mean pressure coefficient, i.e, they are of suction. High mean suctions occur in the band near the roof ridge or the gable end with the maximum mean suction at the ridge/gable end junction.

Figure 3 (b) shows Holmes' results on the same gable roof for the mean pressure coefficient at the 0^0 wind direction (Holmes, 1981). For most of the pressure taps, Holmes' results are similar to the present results. Only a few pressure taps have slightly different values from the present results. This may be due to a slightly different simulation of boundary layer wind in the wind tunnel. A 300 mm high fence was used by Holmes while a 400 mm high fence was used in this study. The comparison between the two independent tests indicates that the pressure measurement system and the flow simulation used in this study are appropriate.

Presented in Fig. 4 is the distribution of mean pressure coefficient on the hip roof for the 0^0 wind direction. All mean wind pressures are negative. High mean suctions occur around the area immediately behind the hip ridge. The hip ridge obviously generates cylindrical vortices, which have been identified as a cause of high suction on roof claddings. The mean suction distribution shown in Fig. 4 is in a manner similar to that found by Meecham et. al. (1991) on a 1:100 scale hip roof model without overhangs. Compared with the mean suctions on the gable roof at the same wind direction, the mean suctions on the hip roof are generally higher and the region of high suction is near the hip ridge. This indicates that roof configuration does affect the magnitude and distribution of mean wind pressures.

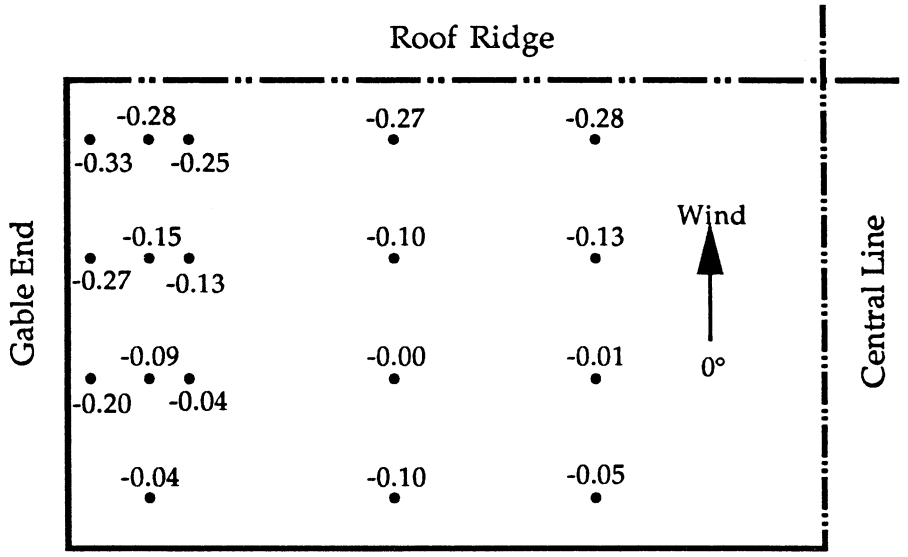

(a) Present Study

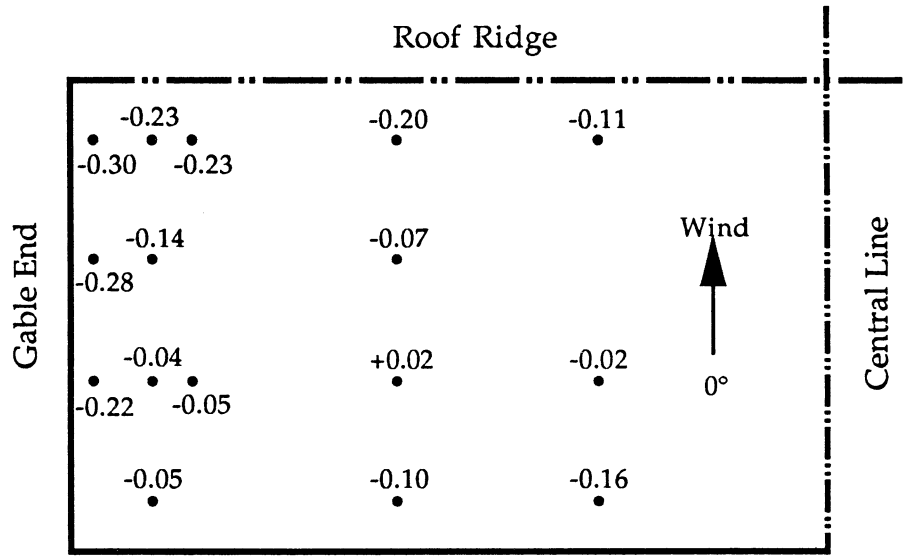

(b) Holmes' Results

FIG.3 DISTRIBUTION OF MEAN PRESSURE COEFFICIENT ON GABLE ROOF FOR A WIND DIRECTION OF 0°

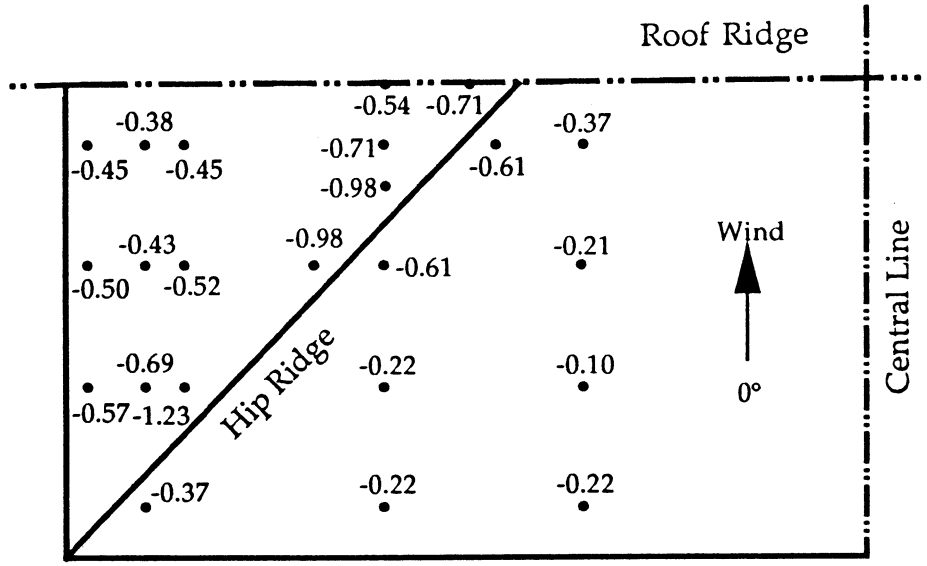

FIG.4 DISTRIBUTION OF MEAN PRESSURE COEFFICIENT ON HIP ROOF FOR A WIND DIRECTION OF 0°

For most of the other wind directions, the situation is reversed. The mean suctions on the hip roof are much less than the gable roof at most of the taps. The largest mean pressure coefficient on the gable roof is - 2.66 at tap 14 for the 135^0 wind direction. The largest mean pressure coefficient on the hip roof is -1.76 at tap 12 for the same wind direction.

3.2 Minimum Peak Pressure Coefficients

The distribution of minimum peak pressure coefficients on the gable roof and its variation with wind direction are shown in Figs. 5(a) to 5(d) for the 0^0, 45^0, 90^0 and 135^0 wind directions, respectively. As the wind is normal to the long wall of the model, high peak suctions occur along the leading edges at both the gable end and front wall with the largest negative peak pressure coefficient of -1.46. When wind direction is 45^0, peak suctions at the gable end become high. The highest peak suction occurs near the gable/ridge junction with the largest negative peak pressure coefficient of -3.65. For a wind direction of 90^0, i.e., the wind normal to the gable end, higher peak suctions distribute over a relatively large area near the gable end with the largest negative peak pressure coefficient of -4.59 in this direction. The measured worst suction for all concerned pressure taps and wind directions was found at tap 14 for a wind direction of 135^0 with the largest negative peak pressure coefficient of -7.00. Both the magnitude and location of the worst suction are almost the same as those found by Holmes (1981).

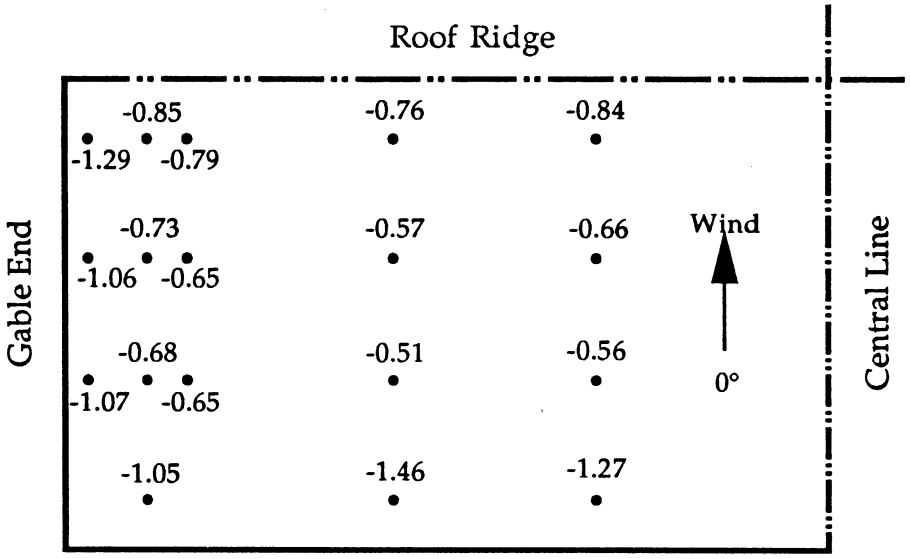

(a) 0° Wind Direction

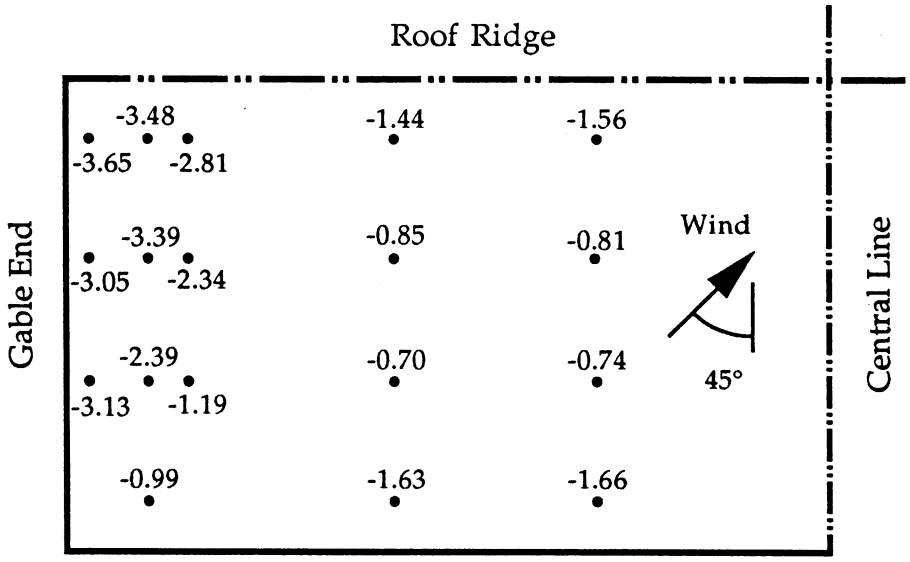

(b) 45° Wind Direction

FIG.5 DISTRIBUTION OF MINIMUM PRESSURE COEFFICIENT ON GABLE ROOF

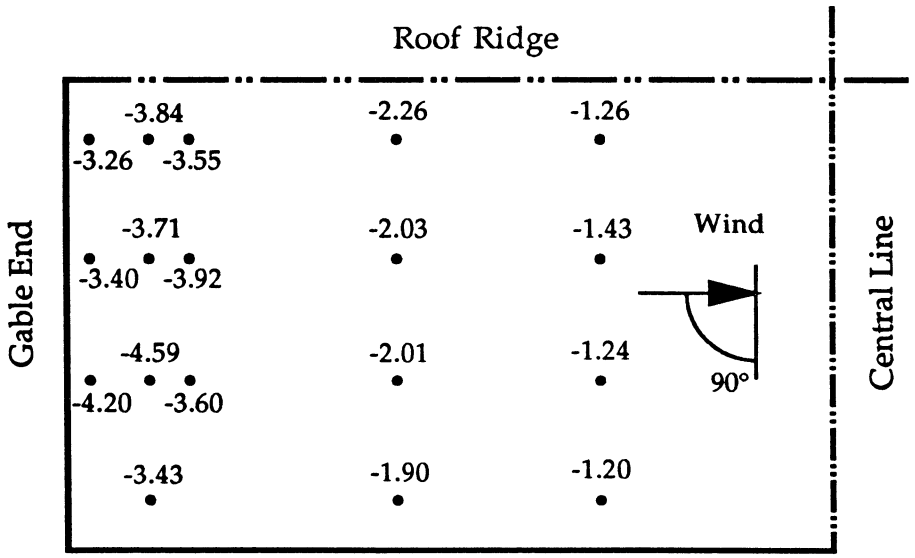

(c) 90° Wind Direction

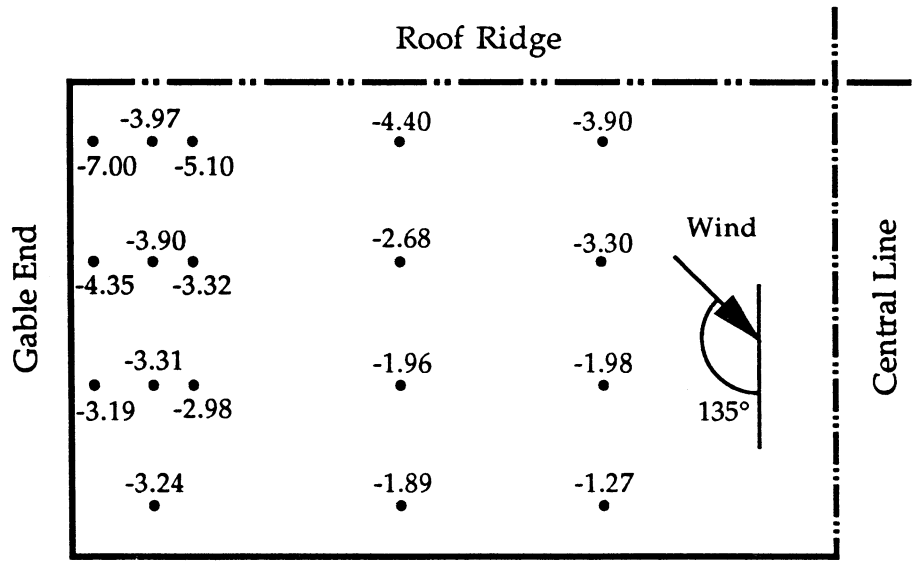

(d) 135° Wind Direction

FIG.5 DISTRIBUTION OF MINIMUM PRESSURE COEFFICIENT ON GABLE ROOF

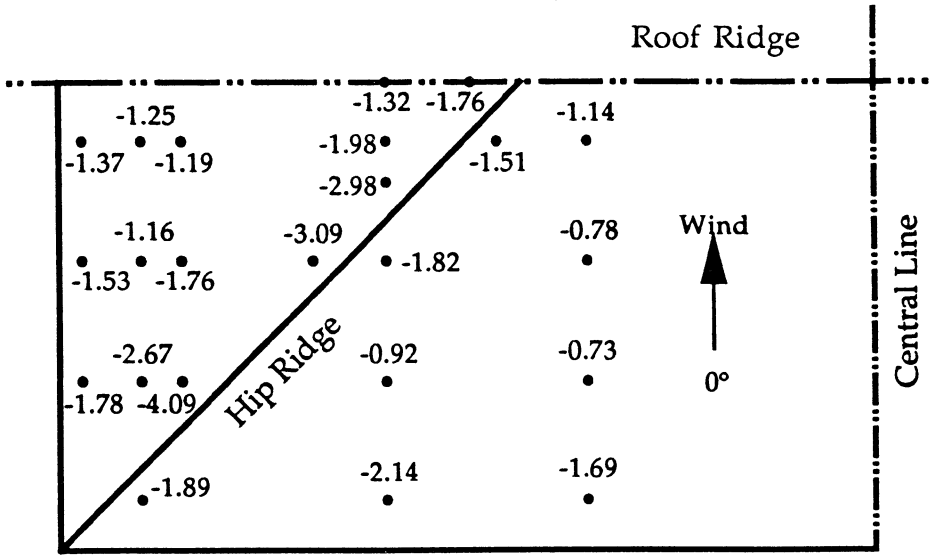

(a) 0° Wind Direction

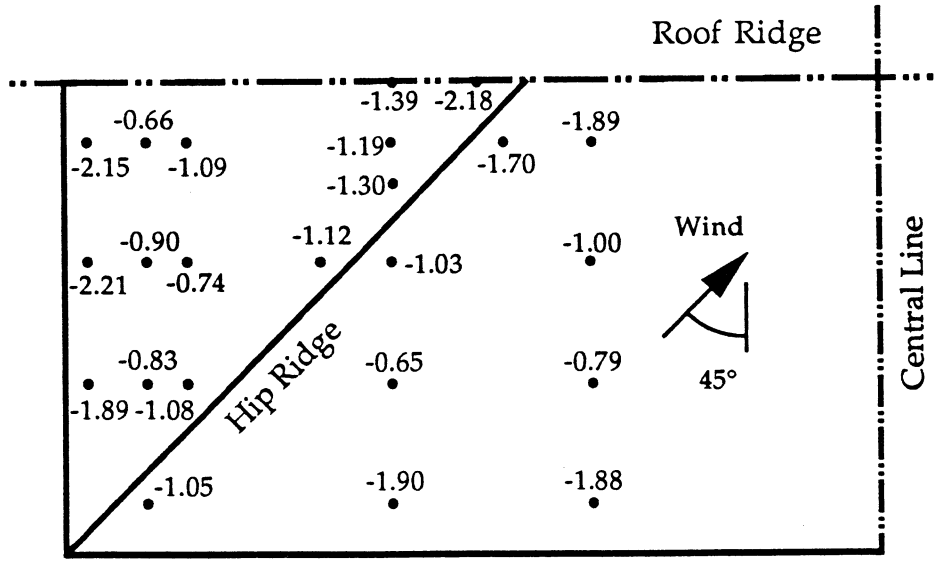

(b) 45° Wind Direction

FIG.6 DISTRIBUTION OF MINIMUM PRESSURE COEFFICIENT ON HIP ROOF

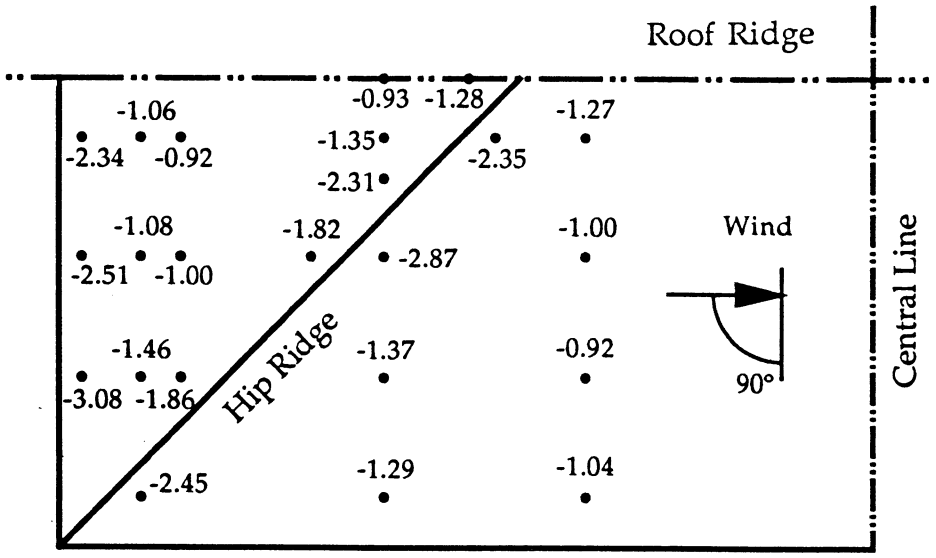

(c) 90° Wind Direction

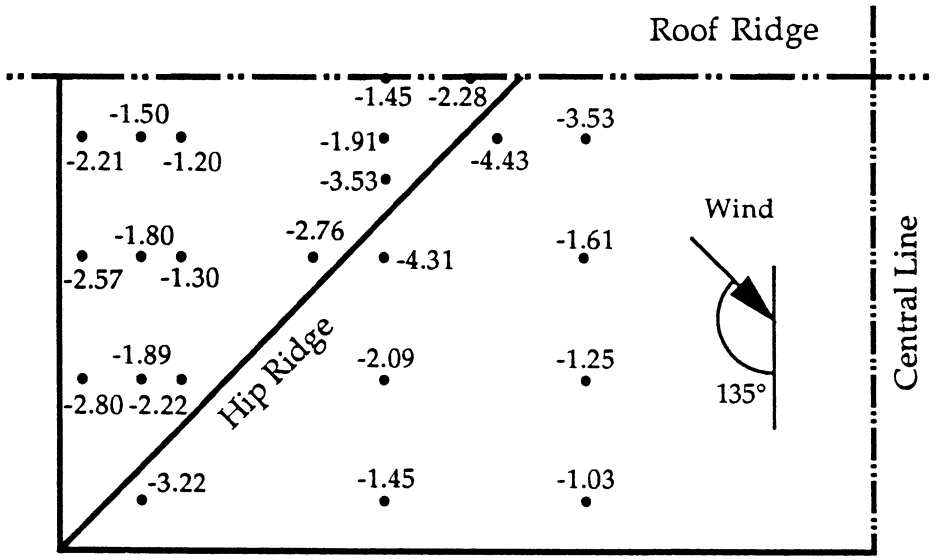

(d) 135° Wind Direction

FIG.6 DISTRIBUTION OF MINIMUM PRESSURE COEFFICIENT ON HIP ROOF

Presented in Figs. 6(a) to 6(d) are the distributions of minimum peak pressure coefficients on the hip roof for the 0^0, 45^0, 90^0 and 135^0 wind directions, respectively. At the 0^0 wind direction, tap 6, which has the highest mean suction in this direction, also has the highest peak suction with the largest negative peak pressure coefficient of -4.09. When wind direction is 45^0, the peak suctions near the hip edge increase moderately but the peak suctions around the hip ridge reduce significantly in comparison with the 0^0 wind direction. This is because the wind flow now is parallel to the hip ridge and no significant vortices occurs near the hip ridge. The largest negative peak coefficient is only -2.21 at tap 9 in the 45^0 wind direction. With the wind normal to the hip edge (i.e., the 90^0 wind direction), the largest negative peak pressure coefficient in this direction is -3.08 at tap 4. At the 135^0 wind direction, the air flow becomes normal to the hip ridge. High peak suctions take place just behind the leading edge of the hip ridge with the largest negative peak pressure coefficient of -4.43 at tap 21. The measured worst suction for all concerned taps and wind directions was found at tap 21 at a wind direction of 120^0 with the largest negative peak pressure coefficient of -4.63.

Comparing the minimum peak pressure coefficients on the hip roof with those on the gable roof, one can find that at the 0^0 wind direction peak suctions are generally higher on the hip roof than on the gable roof, but at most of the other wind directions peak suctions are much lower on the hip roof than on the gable roof. In particular, the largest negative peak pressure coefficient in all the taps tested and all the wind directions concerned is -7.00 for the gable roof but only -4.63 for the hip roof. The location of the largest negative peak pressure on the gable roof is near the gable/ridge junction, but on the hip roof it is just behind the hip ridge.

The worst (largest) negative peak pressure coefficient of each tap in all the concerned wind directions is shown in Fig. 7(a) for the gable roof and Fig. 8(a) for the hip roof. The corresponding critical wind direction for each tap is given in Fig. 7(b) for the gable roof and Fig. 8(b) for the hip roof. It is clear that for the gable roof, high peak suctions occur along the leading edges at both the gable end and roof ridge but for the hip roof, high suctions occur around the hip ridge. The magnitudes of peak suctions on the hip roof are much smaller than those on the gable roof. These differences may explain the disparity in the static performance of hip and gable roof claddings during strong winds, as observed in some post disaster investigations.

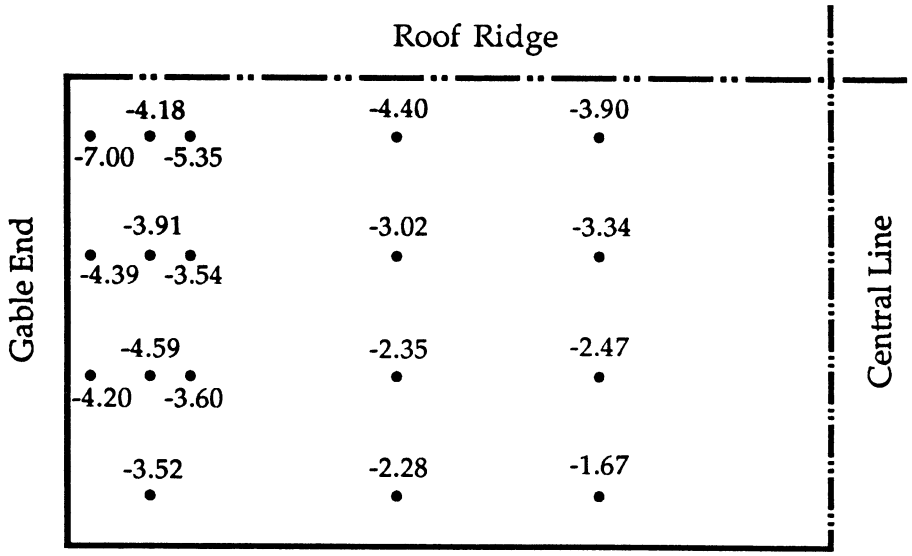

(a) Worst Negative Peak Pressure

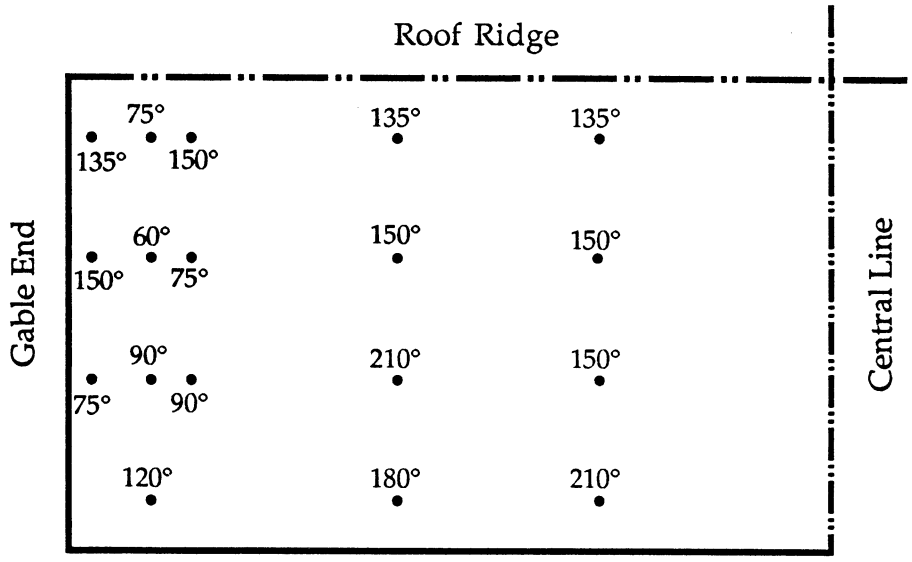

(b) Critical Wind Direction

FIG.7 WORST NEGATIVE PEAK PRESSURE COEFFICIENTS AND CRITICAL WIND DIRECTIONS FOR GABLE ROOF

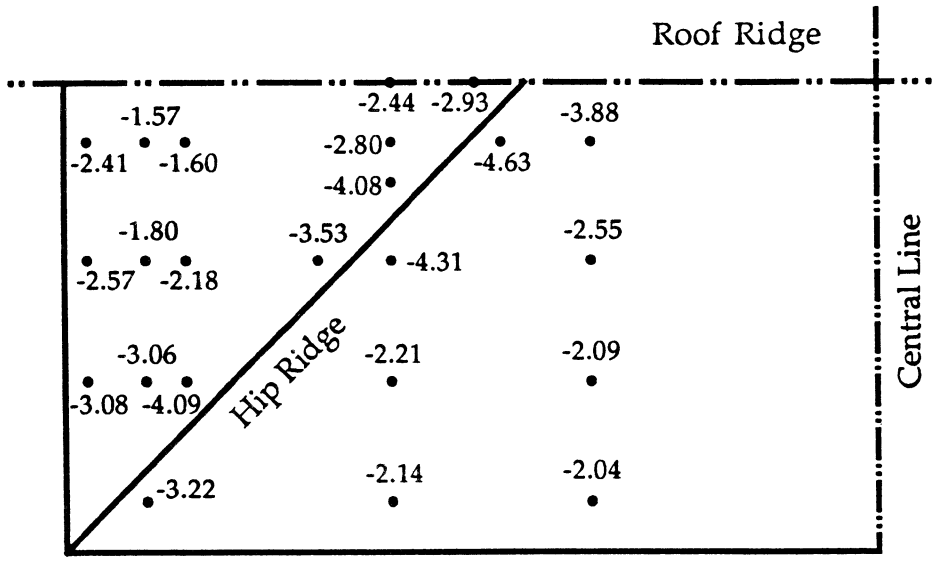

(a) Worst Negative Peak Pressure

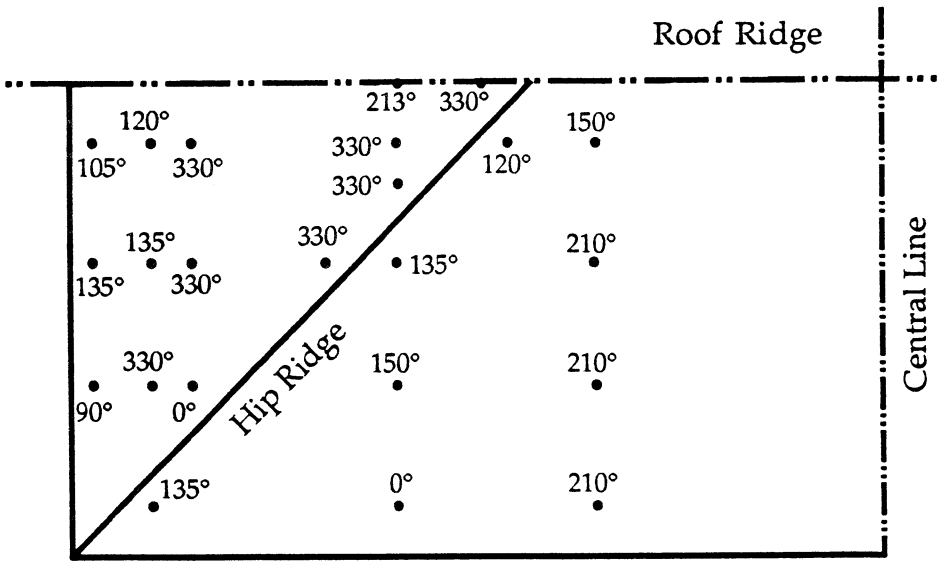

(b) Critical Wind Direction

FIG.8 WORST NEGATIVE PEAK PRESSURE COEFFICIENTS AND CRITICAL WIND DIRECTIONS FOR HIP ROOF

4 COMPARISON OF FATIGUE CHARACTERISTICS

To determine fatigue characteristics and fatigue damage to steel roof claddings, the pressure time-histories were recorded for each tap at its critical wind direction. Fatigue characteristics of a roof pressure consist of three elements: the minimum peak pressure coefficient in one record or the maximum peak pressure coefficient range (the maximum peak pressure coefficient minus the minimum peak pressure coefficient); the number of cycles; and cycle histogram. Based on these elements and information on wind climate, the total fatigue loading at each tap can be estimated. Several count methods are available at present to determine the elements. A study carried out by Xu (1995a) shows that the rainflow count method is probably the most suitable method for roof pressures.

4.1 Rainflow Count Method

In practice, there are several equivalent definitions of the rainflow count method. The following rules for operating the rainflow count method have been described by Fuchs and Stephens (1980):

1. Rearrange the history to start with the highest peak.
2. Start from the highest peak and go down to the next reversal (see Fig. 9). Proceed horizontally to the next downward range; if there is no range going down from the level of the valley at which you have stopped, go upward to the next reversal.
3. Repeat the same procedure upward instead of downward and continue these steps to the end.
4. Repeat the procedure for all the ranges and parts of a range that were not used in previous procedures.
5. If the lowest valley is more extreme than the highest peak, start with the lowest valley and go up instead of down.

By using these rules, four cycles can be identified from the sample history shown in Fig. 9. These four cycles are 1-2-4-5-6-11-12, 2-3-4, 6-7-9-10-11 and 7-8-9. The range and mean of each cycle can be determined using the coordinates of the corresponding peak and valley. For instance, the range of the cycle 2-3-4 is p_3-p_2, and the mean of the cycle is $\frac{1}{2}(p_3+p_2)$.

It is clear that the rainflow count method can identify cycles as closed hysteresis loops and provide a mean value for each cycle. A hysteresis threshold can be easily set for the size of cycle range to eliminate small

cycles which contribute little to fatigue damage. The load cycles identified by the rainflow method are also compatible with a large quantity of metal roof fatigue data (e.g. S-N curves) from constant-amplitude fatigue tests. However, the rainflow method gives no information about original load cycle sequence, which may have a pronounced influence on the fatigue life estimation of metal roofs. This issue has been discussed in Xu (1995b). It is also extremely difficult to formulate probability equations for cycle ranges and cycle means counted by the rainflow method. As a result, the rainflow method is generally used together with numerical computation.

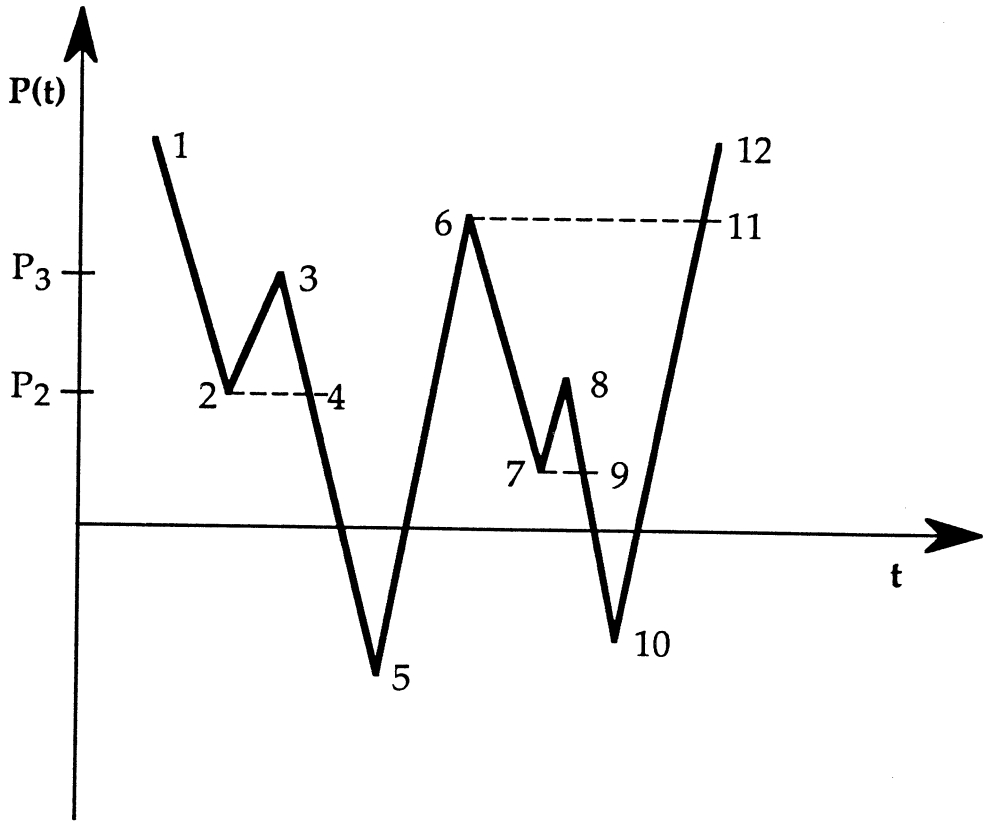

FIG.9 RAINFLOW COUNTING

4.2 Number of Cycles

A Fortran program has been written and used to count load cycles of wind pressures. All the recorded roof pressure time-histories are of the same time duration. To be a reasonable comparison of the number of cycles, the same hysteresis threshold should be employed for all the hip and gable roof pressures. It was decided to use a 5 percentage of the largest peak pressure coefficient range in all the concerned taps and wind directions as the hysteresis threshold. Using the maximum peak pressure coefficient range

rather than the minimum peak pressure coefficient is to consider effects of positive peak pressures at some taps, though they are small compared with negative peak pressures. The largest peak pressure coefficient range in all the concerned wind directions and taps on the two roofs is 6.66 at tap 14 on the gable roof.

By applying the rainflow count method and the same hysteresis threshold to pressure time-histories, the number of cycles for each tap was counted. The obtained number of cycles was then converted to the number of cycles in full scale using the following equation, derived based on the similarity of the Strouhal Number:

$$\frac{N_p}{\bar{u}_{rp} t_p} = \frac{N_m}{\bar{u}_{rm} t_m} \frac{L_m}{L_p} \tag{2}$$

where N = the number of cycles; L = the geometric length; t= the time; and the subscripts p and m stand for prototype and model, respectively.

The number of cycles per hour per m/s of the mean longitudinal speed at the eaves height in full scale is given in Fig. 10(a) for the gable roof and Fig. 10(b) for the hip roof. It is seen that for each type of roof, the number of cycles varies with pressure tap location. As far as the gable roof is concerned, tap 18 has the largest number of cycles but its peak pressure coefficient range is of medium level. Tap 14 has the largest peak pressure coefficient range but its number of cycles is in the third largest. For the hip roof, tap 4 has the largest number of cycles while tap 18 has the smallest number of cycles. The taps around the hip ridge of high suctions however have the numbers of cycles of medium level only. It is clear that the hip roof has a different distribution of the number of cycles from the gable roof.

4.3 Cycle Histogram

The distribution of load cycles over cycle range and mean level can be described by a three dimensional cycle histogram. Figures 11(a) and 11(b) show the cycle distributions of taps 14 and 18 on the gable roof, respectively. The horizontal and lateral coordinates represent the ratio of the range or mean level of cycles to the largest peak pressure coefficient range using a positive sign instead of the actual sign. The vertical axis shows the number of cycles. If the number of cycles in each cell is divided by the total

number of cycles summed from all the cells, the cycle distribution becomes a cycle histogram used to calculate total fatigue loading later. For the sake of clear comparison of the number of cycles and their distribution between the taps, this section uses a form of cycle distribution other than cycle histogram.

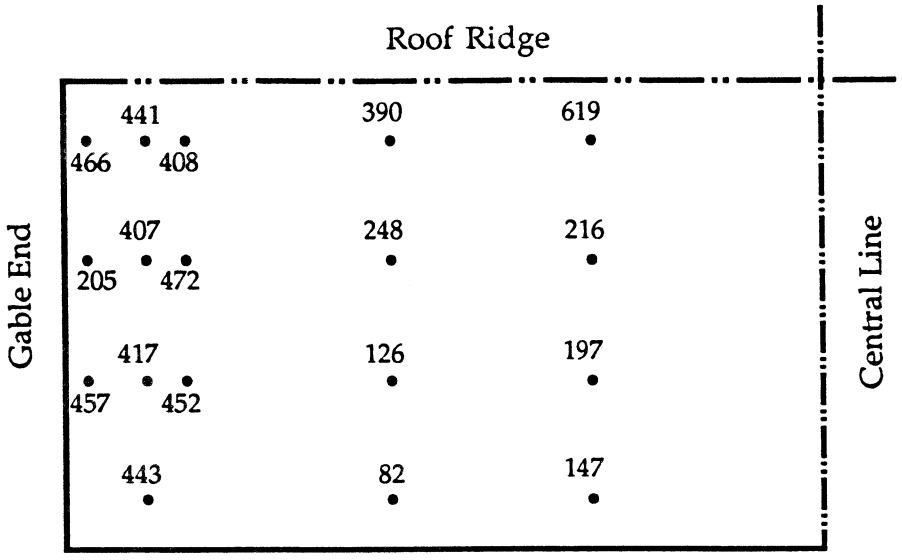

(a) Gable Roof

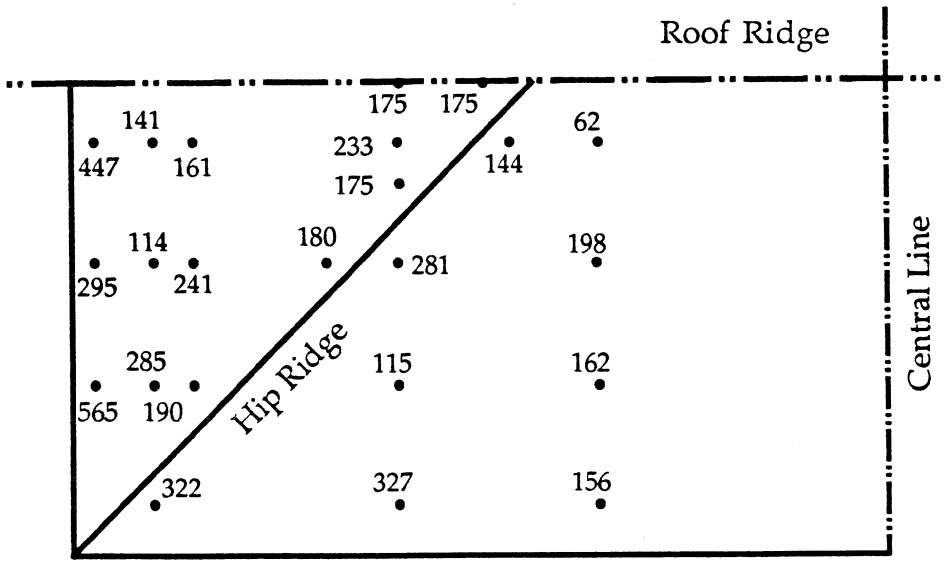

(b) Hip Roof

FIG.10 THE NUMBERS OF CYCLES PER UNIT AT CRITICAL WIND DIRECTION

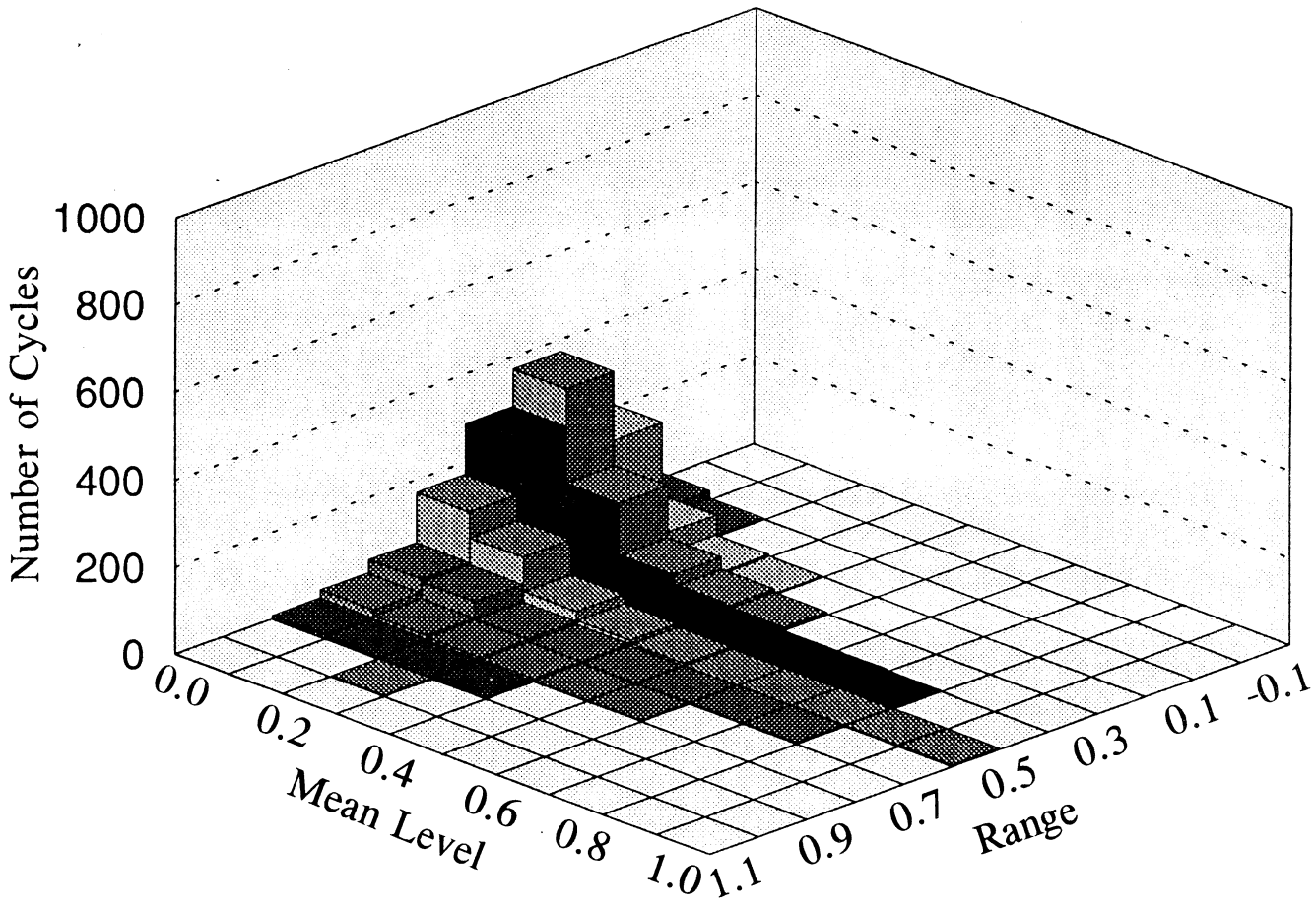

(a) Tap 14

FIG.11 CYCLE DISTRIBUTIONS ON GABLE ROOF

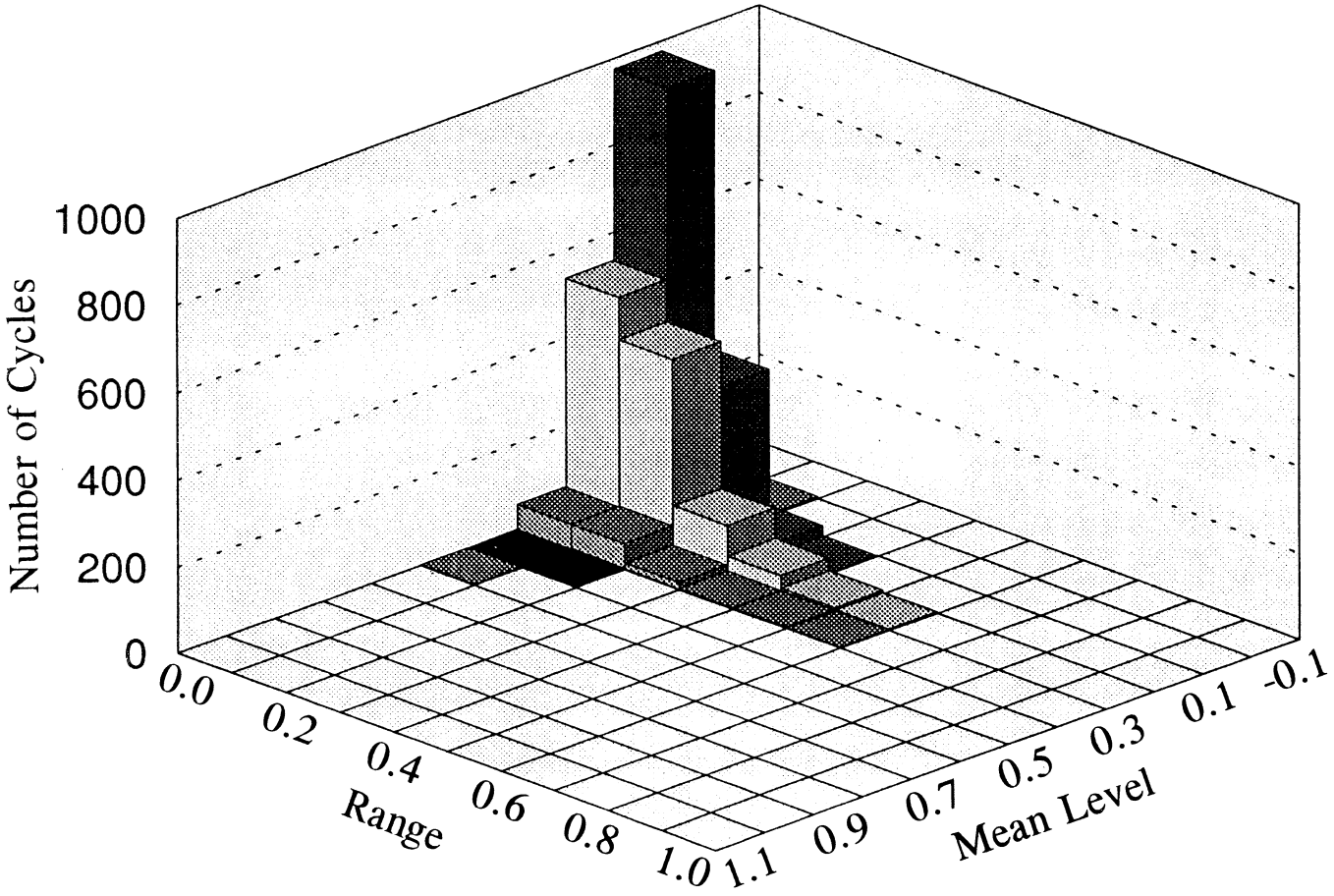

(b) Tap 18

FIG.11 CYCLE DISTRIBUTIONS ON GABLE ROOF

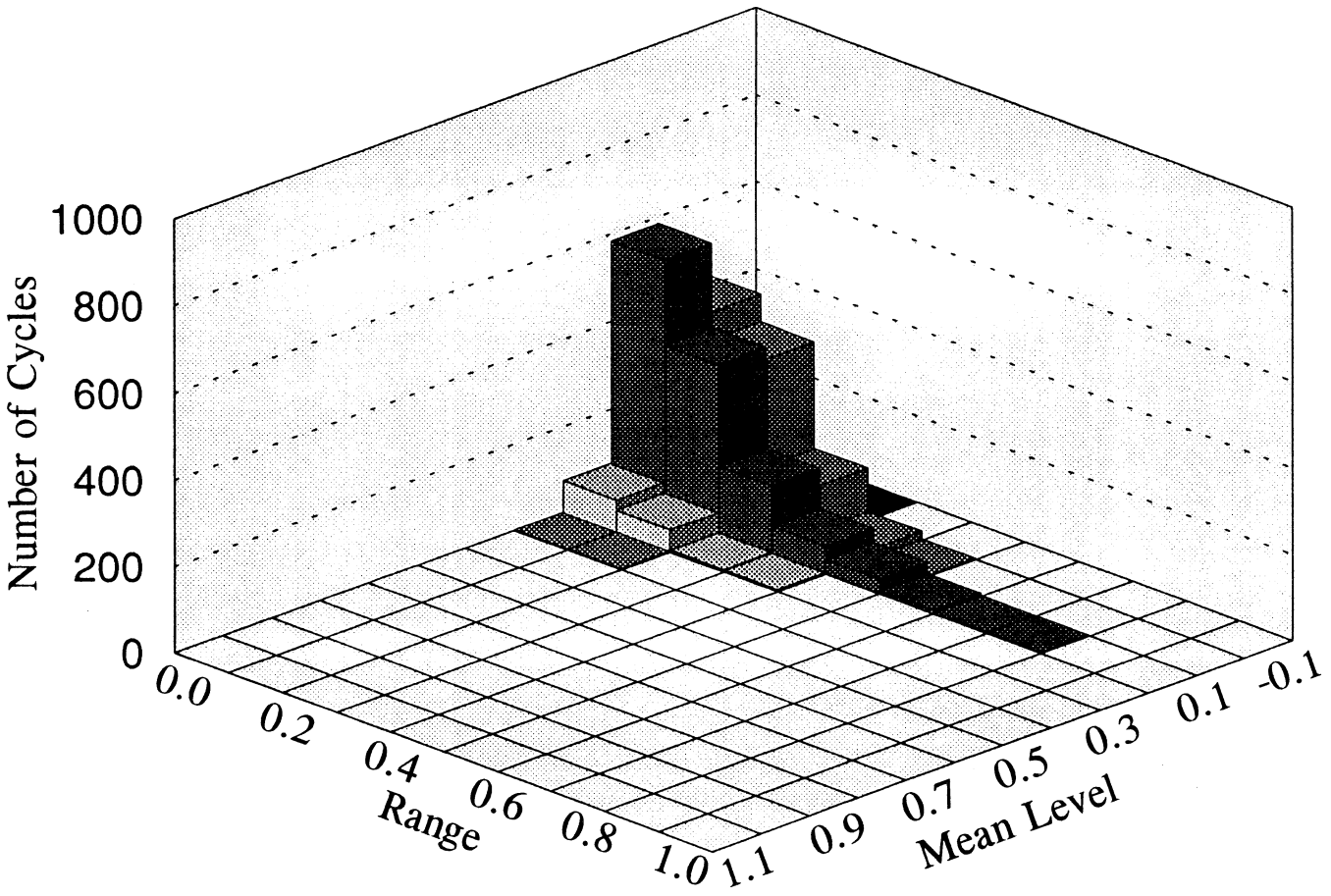

(a) Tap 4

FIG.12 CYCLE DISTRIBUTIONS ON HIP ROOF

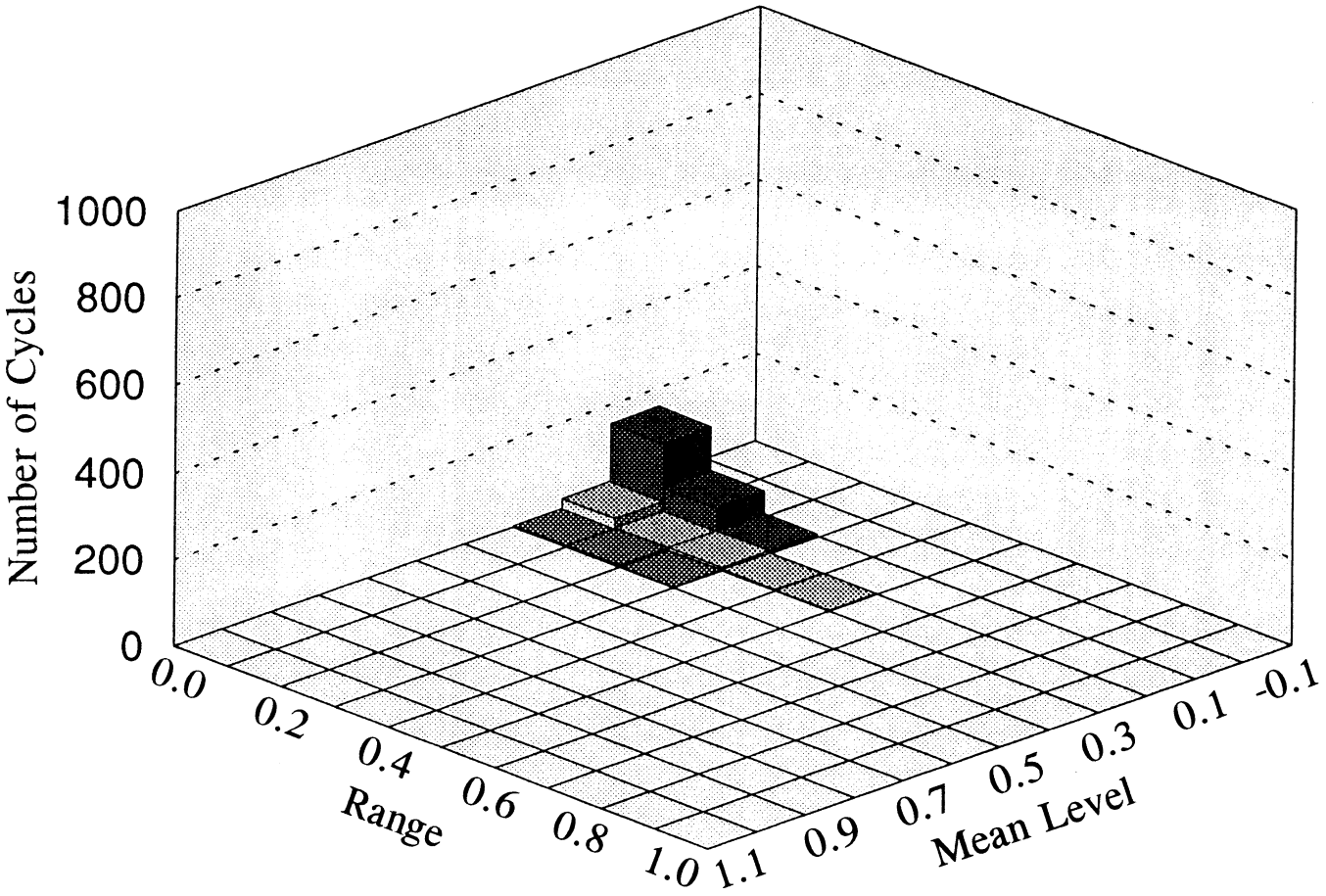

(b) Tap 18

FIG.12 CYCLE DISTRIBUTIONS ON HIP ROOF

It is noted from Figs. 11(a) and 11(b) that there are considerable differences in the cycle distribution. Tap 18 has the largest number of cycles, but most of the load cycles are concentrated on the cells of lower cycle ranges and mean levels. No load cycle range exceeds 70% of the largest peak pressure coefficient range. The cycle distribution of tap 14 extends over more cells including those of higher cycle ranges and mean levels. Load cycles of higher cycle ranges and mean levels would cause more fatigue damage to steel roof claddings than those of lower cycle ranges and mean levels with the same number of cycles.

Presented in Figs. 12(a) and 12(b) are the cycle distributions for taps 4 and 18 on the hip roof, respectively. Only a few load cycles are at tap 18, all of which are concentrated on the cells of lower cycle ranges and mean levels. By contrast, tap 4 has more load cycles and some of them have higher cycle ranges.

The preceding discussions reveal that roof configuration affects not only the largest negative peak pressure but also the number of cycles and cycle distribution. It is also demonstrated that even on the same roof, the number of cycles and cycle distribution would be different at different location.

5 COMPARISON OF FATIGUE DAMAGE

5.1 Total Load Cycle Distribution

Fatigue characteristics of wind pressures, as identified above, together with information on wind climate can be used to determine the total fatigue loading for each tap. The detailed procedure of determining the total fatigue loading can be found in Xu (1995a). Since the present study is mainly a comparative study, one cyclone of 70 m/s gust wind speed and 3-hours duration is considered here as a simple case to calculate the total fatigue loading distribution at each tap on both roofs. Both the buildings are assumed to be located in Cyclonic Region C, as specified by the Australian Wind Loading Code (SAA, 1989).

Only the total load cycle distribution at tap 14 on the gable roof is shown in Fig. 13 as a typical example. The horizontal and lateral coordinates represent the ratio of the range or mean level of cycles to the largest wind pressure range. The largest wind pressure range is equal to 0.5 times the air density times the largest peak pressure coefficient range times the design wind speed. The vertical axis shows the number of cycles generated by the

cyclone. All load cycles are classified into a number of groups, each of which has a constant cycle range and mean level proportional to the largest wind pressure range. As a result, the fatigue damage caused by the specified cyclone can be predicted using the total load cycle distribution in conjunction with fatigue test results of steel roof sheetings under constant-amplitude and variable-amplitude repeated loads.

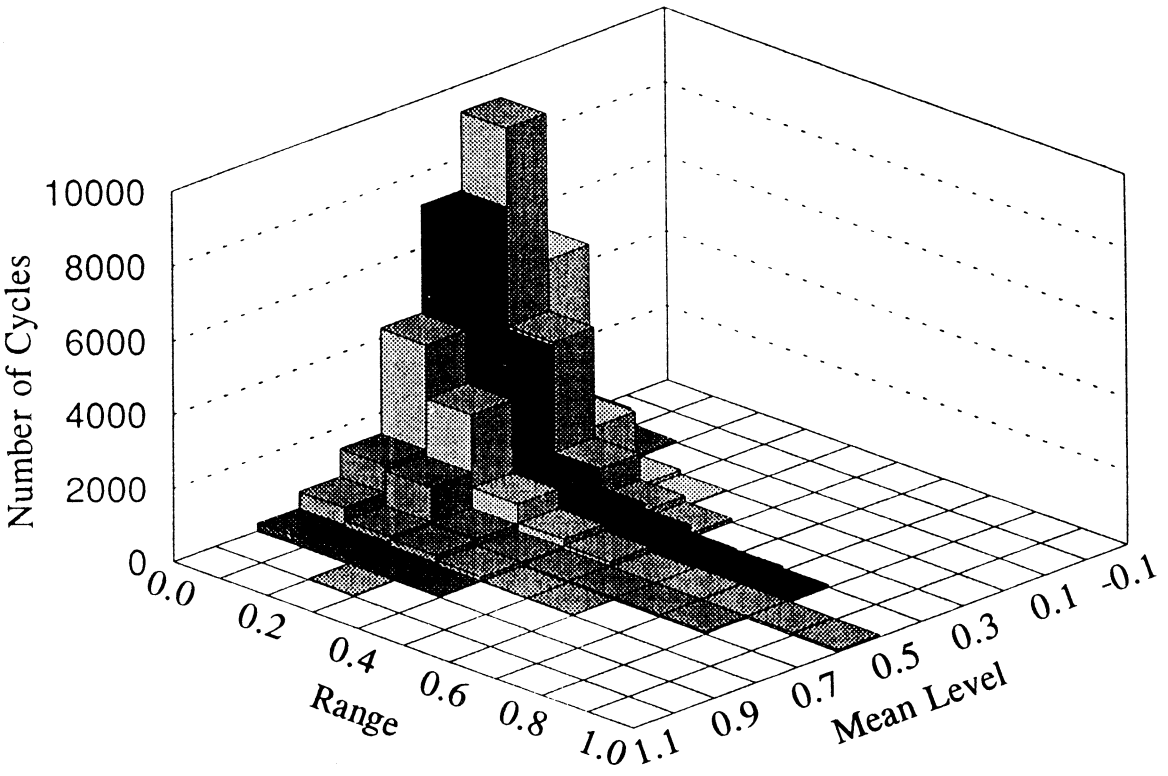

FIG.13 TOTAL LOAD CYCLE DISTRIBUTION AT TAP 14 ON GABLE ROOF

5.2 Fatigue Damage Estimation

Two-span roof assemblies constructed by screw-fastening light-gauge steel roofing sheets of different profiles to high quality timber battens have been tested under both constant and variable-amplitude repeated loads to determine S-N curves of roof sheetings and loading sequence effects on fatigue damage accumulation (Xu, 1995b). The profiles of test roof sheetings were arc-tangent, trapezoidal and ribbed, as shown in Fig. 14. The regression on the test data gave the following two S_{rc}-N curves for the arc-tangent type of roof sheetings:

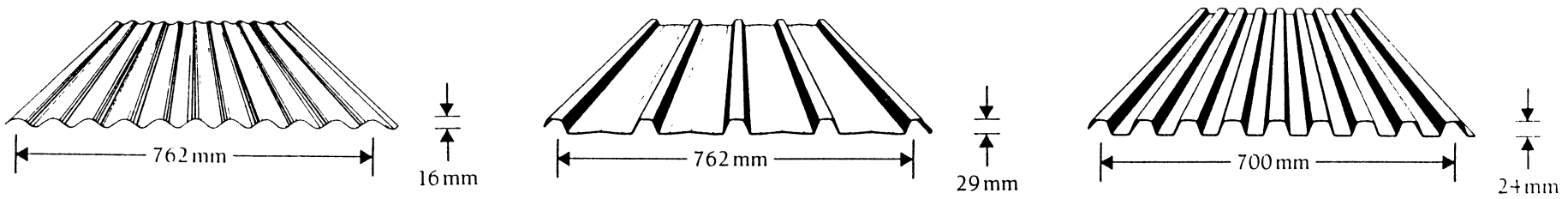

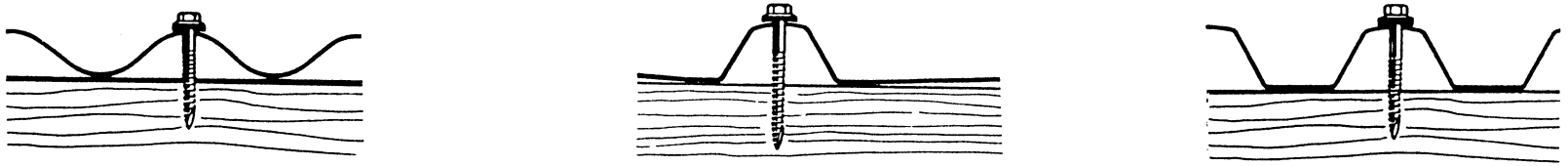

Arc-Tangent Type Sheet

Ribbed Type Sheet

Trapezoidal Type Sheet

FIG. 14 ROOFING SHEETS AND FASTENERS USED IN FATIGUE TESTS

$$N=2.967x10^{7}S_{re}^{-5.624} \qquad S_{re}\leq 6.8 \tag{3a}$$

$$N=4.229x10^{3}S_{re}^{-0.984} \qquad S_{re}>6.8 \tag{3b}$$

The S-N curves for the trapezoidal and ribbed types of roof sheetings are Eq.4 and Eq.5, respectively.

$$N=6.248x10^{5}S_{re}^{-3.008} \tag{4}$$

$$N=2.088x10^{5}S_{re}^{-2.531} \tag{5}$$

In the above equations, N = the number of cycles to failure under S_{re}; and S_{re} = the equivalent load cycle range with zero mean level in kPa. S_{re} is determined through the Goodman model.

$$\frac{S_r}{S_{re}}+\frac{S_m}{S_u}=1 \tag{6}$$

in which S_r = the load cycle range; S_m = the mean level of load cycle; and S_u = the ultimate load obtained from static tests of roofing sheets.

Since the Miner's rule could not well predict fatigue damage of screw-fastened roofing sheets and sheeting profiles did affect the mechanism of fatigue damage accumulation, a modified Miner's rule was suggested.

$$D=\sum_{i}^{m}\frac{n_i}{KN_i} \tag{7}$$

where n_i = the total number of cycles in the ith block of constant load cycle range S_{rei}; N_i = the number of cycles to failure under S_{rei}; m = the total number of blocks; and the K = the modifying factor. Failure occurs when fatigue damage index $D \geq 1$.

The modifying factor should be determined from systematic random fatigue tests using measured wind pressure records, but this is not available now. A K value of 0.25 for the arc-tangent type and a K value of 0.64 for the trapezoidal and ribbed types of sheetings could be used as an

approximation, based on the variable-amplitude repeated load test results.

Using the total load cycle distribution and the above equations, one can calculate fatigue damage index for each tap for each type of roof sheeting. The practical arrangement of roof sheetings at the taps is not considered.

Figures 15(a) and 15(b) show the distributions of fatigue damage index over the gable and hip roofs for the trapezoidal type of sheeting. It is seen that for the gable roof, the maximum damage index is at tap 14 with a value of 0.64 while tap 18 has a fatigue damage index of 0.20 only. The areas having large fatigue damage indexes are near the gable end and roof ridge, where high negative peak pressures were found.

For the hip roof, the maximum damage index is at tap 4 with a value of 0.28. It is only 44% of the maximum damage index on the gable roof. Along the both sides of the hip ridge, where high negative peak pressures were found, the fatigue damage indexes are of medium levels only. This indicates that high fatigue damage indexes may not be at the places of high negative peak pressures.

Presented in Figs. 16(a) and 16(b) are the distributions of fatigue damage index on both roofs for the arc-tangent type of roof sheeting. The maximum fatigue damage index for the gable roof is 1.57 at tap 14 while the maximum fatigue damage index for the hip roof is 0.12 only at tap 4. The fatigue damage index of 1.57 means the failure of the roof sheeting. Since the fatigue damage index at tap 14 on the gable roof is 0.64 and the fatigue damage index at tap 4 on the hip roof is 0.28 for the trapezoidal type of roof sheeting, effects of types of roof sheeting on fatigue damage are obvious.

Figures 17(a) and 17(b) show the distributions of fatigue damage index on both roofs for the ribbed type of roof sheeting. The maximum fatigue damage index on the gable roof is 1.47 at tap 4 while the maximum fatigue damage index on the hip roof is 0.69 at tap 4. Effects of types of roof sheeting on fatigue damage are evidenced again.

6 CONCLUSIONS

The comparison of wind pressures, fatigue loading and fatigue damage to roof claddings on the hip and gable roof buildings of a 20^0 roof slope has been carried out through wind tunnel tests and computer analyses.

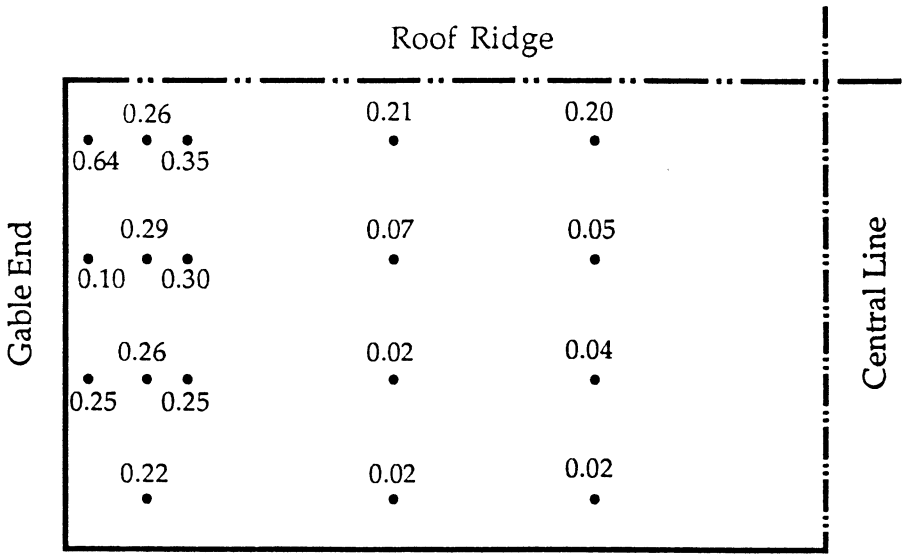

(a) Gable Roof

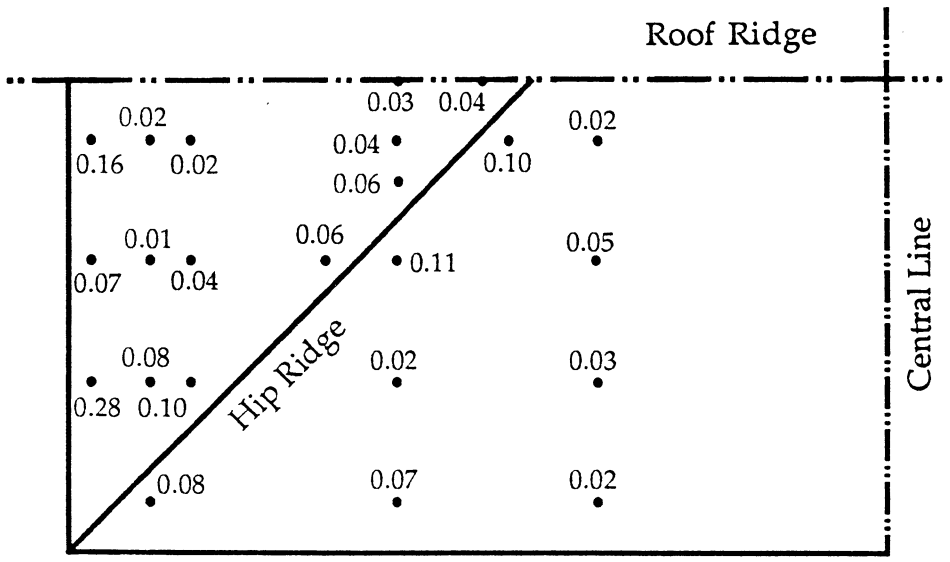

(b) Hip Roof

FIG. 15 FATIGUE DAMAGE INDEXES OF TRAPEZOIDAL ROOF SHEETING

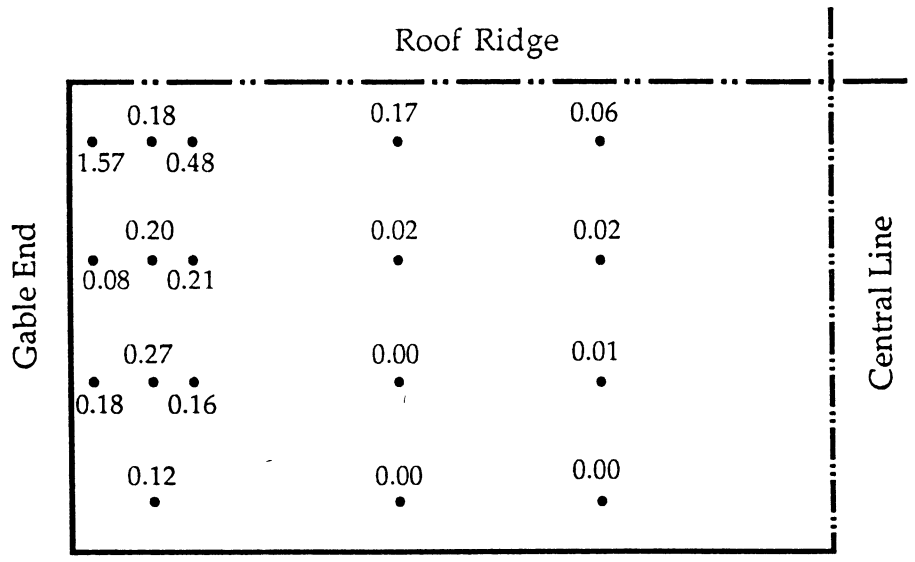

(a) Gable Roof

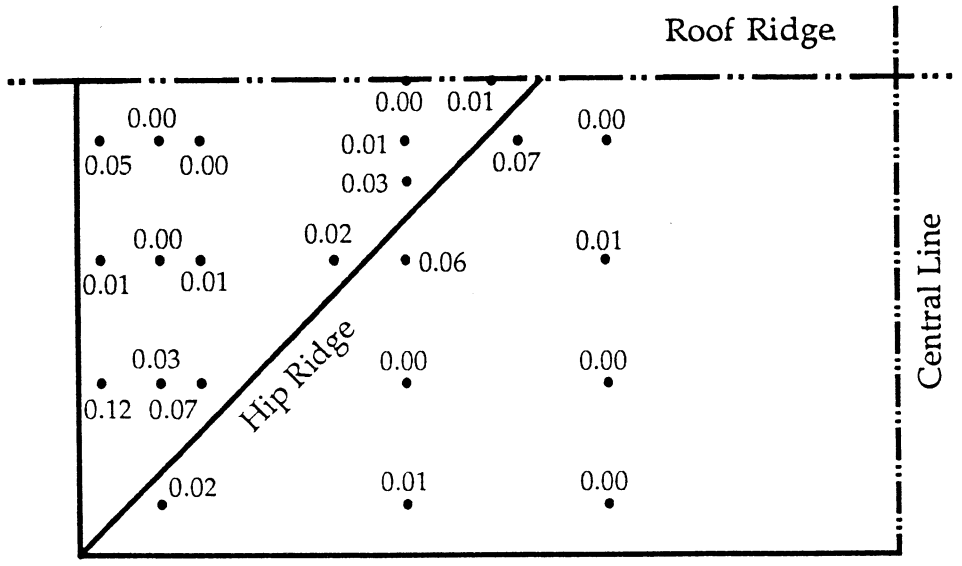

(b) Hip Roof

FIG. 16 FATIGUE DAMAGE INDEXES OF ARC-TANGENT ROOF SHEETING

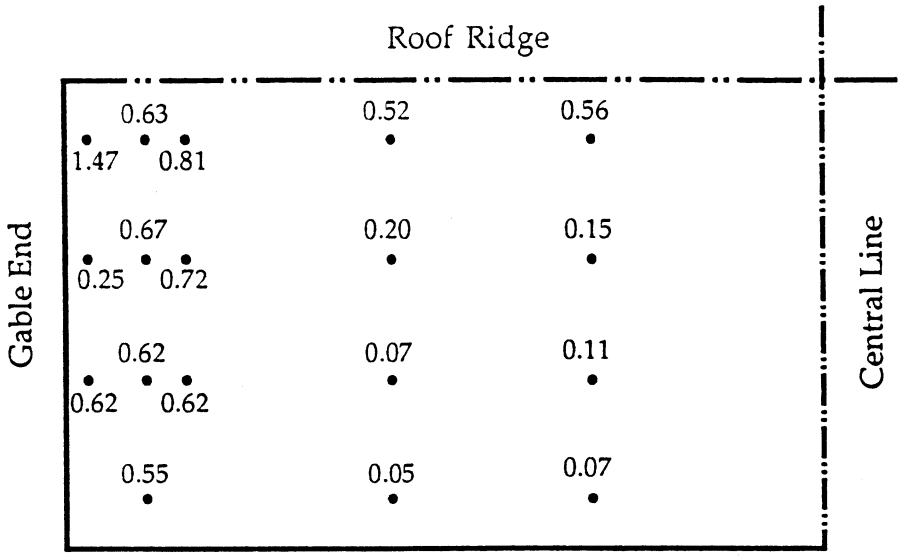

(a) Gable Roof

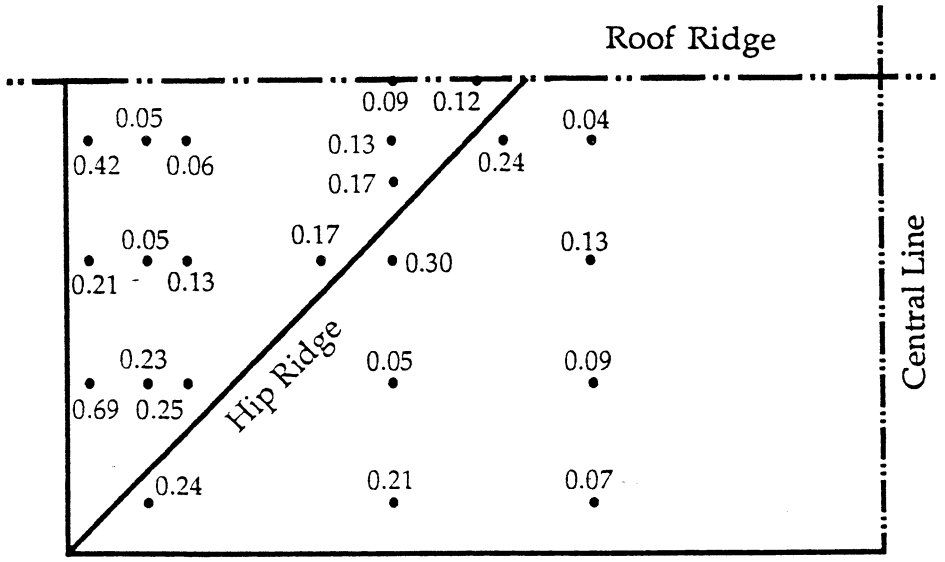

(b) Hip Roof

FIG. 17 FATIGUE DAMAGE INDEXES OF RIBBED ROOF SHEETING

The gable roof suffered the worst suction at the gable/ridge junction with a peak coefficient of -7 while the hip roof suffered the worst suction at the hip ridge with a peak coefficient of -4.6. Wind suctions on most parts of the hip roof were much less severe than those on the gable roof.

The roof configuration did affect the number of cycles and cycle distribution. The number of cycles and cycle distribution even varied with the location of pressure taps on the same roof configuration. Fatigue damage to roof claddings depended on not only the roof configuration and tap location but also the type of roof sheeting. The distributions of fatigue damage index over both roofs showed that under the same strong winds, fatigue damage to the hip roof cladding was much less severe than that to the gable roof cladding for all three types of roof sheeting. The areas susceptible to fatigue damage were near the gable end and roof ridge for the gable roof, but near the side wall and hip ridge for the hip roof.

Further studies are required for wind pressures and fatigue loading on hip-roofed low-rise buildings of different aspects. An integral investigation of wind loading and structural systems of hip-roofed low-rise buildings is also needed.

7 ACKNOWLEDGMENTS

The writers are grateful to the financial support from Industries and James Cook University. They wish to thank Mr G. McNealy, Senior Technician at the Department of Civil & Systems Engineering, for all his help during the wind tunnel tests.

8 REFERENCES

Fuchs, H.O. and Stephens, R. I. (1980) "*Metal fatigue in engineering*", John Wiley & Sons.

Holmes, J.D. (1980) "*Wind pressures and forces on tropical houses*", Final report of Project No. 17 of the Australian Housing Research Council.

Holmes, J.D. (1981) "Wind pressures on houses with high pitched roofs", *Wind Engineering Report 4/81*, James Cook University, Townsville, Australia.

Meecham, D., Surry, D. and Davenport, A.G. (1991) "The magnitude and

distribution of wind-induced pressures on hip and gable roofs", *Journal of Wind Engineering and Industrial Aerodynamics*, 38, pp.257-272.

SAA (1989) "*AS1170.2 - SAA loading Code, Part 2: wind loads*", Standard Association of Australia.

Sparks, P.R., Hessig, M.L., Murden, J.A. and Sill, B.L. (1988) " On the failure of single-story wood-frame houses in severe storms", *Journal of Wind Engineering and Industrial Aerodynamics,* 29, pp. 245-252.

Walker, G.R. (1975) "*Report on Cyclone Tracy - Effect on Buildings - December 1974*", Vol. 1, Dept. of Housing and Construction, Australia.

Wittenoom, R.A. (1975) "The performance of Western Australian housing structures under cyclone loadings", *the Annual Engineering Conference,* The Institution of Engineers, Australia.

Xu, Y.L. (1995a) "Determination of wind-induced fatigue loading on roof cladding", *Journal of Engineering Mechanics,* ASCE, Vol.121, No.9, Sept..

Xu, Y.L. (1995b) "Fatigue performance of screw-fastened light gauge steel roofing sheets", *Journal of Structural Engineering*, ASCE, Vol.121, No.3, Mar., pp. 389-398.

Xu, Y.L. and G.F. Reardon (1995) "Full-scale and model scale wind pressure and fatigue loading on the Texas Tech University Building", *Technical Report No. 42*, Cyclone Testing Station, James Cook University, Townsville, Australia (in print).